© 2019. This manuscript version is made available under the CC-BY-NC-ND 4.0 license http://creativecommons.org/licenses/by-nc-nd/4.0/
The published version is available via https://doi.org/10.1016/j.ijpharm.2019.119010.

International Journal of Pharmaceutics

Characteristics of unique endocytosis induced by weak current for cytoplasmic drug delivery

Tasuku Torao[1‡], Miyuki Mimura[1‡], Yasufumi Oshima[1‡], Koki Fujikawa[2], Mahadi Hasan[3,4], Tatsuharu Shimokawa[2], Naoshi Yamazaki[4], Hidenori Ando[4], Tatsuhiro Ishida[4], Tatsuya Fukuta[4], Tamotsu Tanaka[4], Kentaro Kogure[4]*

[1]Faculty of Pharmaceutical Sciences, Tokushima University, Tokushima, Japan, [2]Graduate School of Pharmaceutical Sciences, Tokushima University, Tokushima, Japan, [3]JSPS International Research Fellow, Japan, [4]Graduate School of Biomedical Sciences, Tokushima University, Tokushima, Japan

*Corresponding author: Kentaro Kogure, Graduate School of Biomedical Sciences, Tokushima University, Shomachi 1, Tokushima, 770-8505, Japan, kogure@tokushima-u.ac.jp

‡ These authors contributed equally to this work

Abstract

We previously reported that a weak current (WC, 0.3-0.5mA/cm^2) applied to cells can induce endocytosis to promote cytoplasmic delivery of hydrophilic macromolecules (MW: < 70,000), such as dextran and siRNA, which leak from WC-induced endosomes into the cytoplasm (Hasan et al., 2016). In this study, we evaluated the characteristics of WC-mediated endocytosis for application of the technology to cytoplasmic delivery of macromolecular medicines. WC induced significantly higher cellular uptake of exogenous DNA fragments compared to untreated cells; the amount increased in a time-dependent manner, indicating that endocytosis was induced after WC. Moreover, following WC treatment of cells in the presence of an antibody (MW: 150,000) with the lysosomotropic agent chloroquine, the antibody was able to bind to its intracellular target. Thus, high molecular weight protein medicines delivered by WC-mediated endocytosis were functional in the cytoplasm. Transmission electron microscopy of cells treated by WC in the presence of gold nanoparticles covered with polyethylene glycol showed that the WC-induced endosomes exhibited an elliptical shape. In the WC-induced endosomes, ceramide, which makes pore structures in the membrane, was localized. Together, these results suggest that WC can induce unique endocytosis and that macromolecular medicines leak from endosomes through a ceramide pore.

Key words: weak current; cellular uptake; cytoplasmic delivery; endosomal leakiness; ceramide pore; tubular endocytosis

40

1. Introduction

Iontophoresis using weak current (WC; 0.3-0.5 mA/cm^2) is a technology that promote permeation of ionized drug molecules for transdermal drug delivery (Kalia, et al., 2004; Karpiński, 2018). Electric repulsion and electro-osmosis are thought to be the primary mechanisms related to iontophoresis (Kalia, et al., 2004). Molecules that are amenable to iontophoresis are typically ionic, hydrophobic, and exhibit low molecular weights (<10,000). As such, iontophoresis was thought to be unsuitable to promote transdermal delivery of hydrophilic macromolecules such as proteins and nucleic acids.

However, several groups reported the delivery of macromolecules, such as proteins and nucleic acids, by iontophoresis (Hashim, et al., 2010; Liu, et al., 2013; Patel, et al., 2013; Labala, et al., 2017). Hashim et al. succeeded in transdermal delivery of NF-kB decoy oligonucleotides by iontophoresis, and suppression of tumor necrosis factor-a production (Hashim, et al., 2010). Liu, et al. reported the intradermal delivery of oligodeoxynucleotides by combination of a chemical penetration enhancer with iontophoresis (Liu, et al., 2013;). Patel, et al. delivered parvalbumin (MW: ca 12,000) across oral mucosa by iontophoresis (Patel, et al., 2013). Labala, et al. succeeded in the suppression of melanoma tumor by iontophoresis of signal transduction and activator of transcription factor 3 (STAT 3) and imatinib using gold nanoparticles (Labala, et al., 2017).

We previously demonstrated successful iontophoretic delivery of various nucleic acids, such as siRNA (MW: ca.12,000), CpG oligo DNA (MW: ca. 6,600), and liposomes encapsulating insulin into the skin (Kigasawa, et al., 2010; Kigasawa, et al., 2011, Kajimoto, et al., 2011) upon treatment with WC (0.3-0.5 mA/cm^2). WC induced a decrease in the amount of the gap-junction protein connexin Cx43 and depolymerization of actin associated with tight-junction structures (Hama, et al., 2014). These findings indicate that the mechanism of skin penetration of hydrophilic macromolecules is via cleavage of intercellular junctions by WC (Hama, et al., 2014).

We also found that siRNA could be delivered by iontophoresis based on the successful knockdown of target mRNA in skin cells treated with WC (Kigasawa, et al., 2010). This finding suggests that siRNA reaches the cytoplasm of WC-treated skin cells as RNAi reactions occur in the cytoplasmic space. We further found that WC-induced cellular uptake of siRNA is mediated by endocytosis (Hasan, et al., 2016a). In general, following endocytic cellular uptake, unmodified siRNA molecules (MW: ca. 12,000) cannot efficiently escape from conventional endosomes, such as clathrin-coated endosomes and macropinosomes, suggesting that cytoplasmic delivery of siRNA proceeds via an alternative mechanism. In our previous report, 10k FITC-dextran (MW: 10,000) was widely dispersed in the cytoplasm 24 hr after treatment with WC, whereas

70k FITC-dextran (MW: 70,000) remained in the endosomes (Hasan, et al., 2016b). Together, these results suggest that WC-induced endosomes exhibit unique structural properties that allow for leakage of macromolecules having molecular weights <70,000.

To better understand the characteristics of this unique WC-mediated endocytosis, we herein examined the temporal relationship between WC and cellular uptake, intracellular functionality of high molecular weight proteins delivered by WC, and morphological observation of WC-mediated endocytosis. We also sought to elucidate the characteristics of WC-induced endosomes in relation to leakage of macromolecules.

2. Materials and methods

2.1. Materials

Cell lysis buffer and plasmid DNA encoding luciferase (pGL3-C) were purchased from Promega Corporation (Madison, WI). Ag-AgCl electrodes were purchased from 3M Health Care (Minneapolis, MN). Monoclonal anti-ceramide (mouse IgM isotype) was purchased from Sigma-Aldrich Co., Ltd. (St. Louis, MO). Mouse monoclonal antibody against anti-nuclear pore complex protein and goat anti-mouse IgG labeled with Alexa Fluor 488 were obtained from Abcam (Cambridge, UK). Chloroquine was purchased from Nakalai Tesque, Inc. (Kyoto, Japan). The mouse melanoma cell line B16-F1 was obtained from Dainippon Sumitomo Pharma Biomedical Co., Ltd. (Osaka, Japan). Cells were cultured in Dulbecco's modified Eagle's medium (DMEM) supplemented with 10% fetal bovine serum (FBS) at 37 °C in 5% CO_2.

2.2. Preparation of DNA fragments

DNA fragments encoding the luciferase open reading frame region were prepared by PCR using pGL3-C as a template. The PCR primer sequences were: 5'-CCGAAAGGTCTTACCGGAAAACTCG-3' and 5'-TCCAAACTCATCAATGTATCTTATC-3'. PCR was performed using a PrimeScript One

Step RT-PCR Kit Ver. 2 (Takara Co. Ltd., Japan). The PCR products were subjected to 15% agarose gel electrophoresis and the relevant DNA fragments were extracted from the agarose gel using NucleoSpin Gel and PCR Clean-up (Takara Co. Ltd., Japan). The DNA fragment concentration in the extracted solution was determined using a Nanodrop instrument (Thermo Fisher Scientific Inc., Waltham, MA).

2.3. Weak current (WC) treatment of cultured cells

B16-F1 cells ($1x10^5$ cells/well) were cultured in 35-mm dishes for WC treatment. After 18 hr of cell culture, the cells were washed with PBS before 800 μl serum-free DMEM containing DNA fragment (0.5 μg) or antibody (6 μg) was added to the cells. Ag-AgCl electrodes with a 2.5 cm^2 surface area were placed in the dish, and the cells were treated with a constant WC of 0.34 mA/cm^2 for 15 min.

2.4. Quantification of DNA fragments in cells exposed to WC

Following WC treatment with DNA fragments, B16-F1 cells were incubated at 37 °C for 1 hr or 3 hr and cellular DNA was extracted using a GenElute Mammalian Genomic DNA Miniprep Kit (Sigma-Aldrich, St. Louis, MO). The amount of DNA was quantified based on a calibration curve of the DNA fragment amplified using a real-time PCR Thermal

Cycler Dice Real Time System III (Takara Bio Inc., Japan).

2.5. Immunostaining of cells following WC treatment in the presence of anti-nuclear pore complex antibody

Following WC treatment (0.34 mA/cm^2, 15 min), B16-F1 cells were incubated for 3 hr at 37 °C in the presence of anti-nuclear pore complex protein antibody and 0.01 mM chloroquine before 1 ml DMEM containing 10% FBS was added to the cell dish. After 21 hr incubation, the cells were washed with PBS. Then, 0.5 ml of PBS containing 4% paraformaldehyde was added and the cells were incubated for 20 min at room temperature. The cells were washed with PBS containing 1% BSA and 0.1% Triton. After washing, the cells were incubated for an additional 20 min at room temperature in the presence of PBS containing 1% BSA and 0.1% Triton. Goat anti-mouse IgG labeled with Alexa Fluor 488 (1 μg/mL in 1%BSA-0.1%Triton-PBS) was then added to the dish, and the cells were incubated for 60 min at room temperature. After incubation, the cells were washed three times with 1% BSA-0.1% Triton-PBS. Nuclei were stained by incubating the cells for 30 min in the presence of DAPI solution (1 μg/mL in PBS) and the cells were washed with PBS before observation with an LSM700 confocal laser scanning microscope (Carl Zeiss, Germany).

2.6. Transmission electron microscopic observation

B16-F1 cells were treated with WC (0.34 mA/cm^2) for 15 min in the presence of PEGylated gold nanoparticles having a diameter and zeta potential of 100 nm and -50 mV, respectively. Following WC treatment, cells were incubated for 4 hr; the culture medium was then removed and the cells were fixed with 2% paraformaldehyde (PFA) and 2% glutaraldehyde (GA) in 0.1 M phosphate buffer (PB) pH 7.4 at the incubation temperature, before subsequent incubation at 4 °C. Thereafter, the cells were fixed with 2% GA in 0.1 M PB at 4 °C overnight. After fixation, the samples were washed 3 times with 0.1 M PB for 30 min per wash, and post-fixed with 2% osmium tetroxide (OsO4) in 0.1 M PB at 4 °C for 1 hr. The samples were dehydrated in graded ethanol solutions (50%, 70%, 90%, 100%) by incubating for 5 min each in 50% and 70% solutions at 4 °C, in 90% solution for 5 min at room temperature, and 3 changes of 100% ethanol for 5 min each at room temperature. The samples were transferred to Quetol-812 resin (Nisshin EM Co., Tokyo, Japan) and allowed to polymerize for 48 hr at 60 °C. The polymerized resins were cut into ultra-thin, 90 nm sections with an ultramicrotome equipped with a diamond knife (Ultracut UCT; Leica, Vienna, Austria). The sections were mounted on copper grids that were stained with 2% uranyl acetate at room temperature for 15 min, and then washed

with distilled water followed by secondary staining with lead stain solution (Sigma-Aldrich Co., Tokyo, Japan) at room temperature for 3 min. The grids were observed by transmission electron microscopy (JEM-1400Plus; JEOL Ltd., Tokyo, Japan) at an acceleration voltage of 80 kV. Digital images (2048 x 2048 pixels) were taken with a CCD camera (VELETA; Olympus Soft Imaging Solutions GmbH, Münster, Germany).

2.7. Immunostaining of cells following WC treatment for detection of intracellular distribution of ceramide

Following treatment with WC (0.34 mA/cm^2, 15 min), B16-F1 cells were incubated for 24 hr at 37 °C. The cells were then washed with PBS. PBS (0.5 ml) containing 4% PFA was added and the cells were incubated for 20 min at 37 ºC. The cells were washed three times with PBS containing 1% BSA and 0.1% Triton. After washing, the cells were incubated for an additional 20 min at 37 ºC in the presence of PBS containing 1% BSA and 0.1% Triton. Then, the cells were washed with PBS containing 1% BSA. PBS containing 1% BSA and the primary antibody (mouse anti-ceramide IgM) was added to the cells, and the cells were incubated for 1 hr at 37 ºC. Following that, the cells were washed three times with PBS containing 1% BSA. Goat anti-mouse IgG labeled with Alexa Fluor 488 in 1%BSA-0.1%Triton-PBS was then added to the dish, and the cells

were incubated for 1 hr at 37 °C. After incubation, the cells were washed three times with 1% BSA-0.1% Triton-PBS. Nuclei were stained by incubating the cells for 30 min in the presence of DAPI solution, and the cells were washed with PBS before observation with an LSM700 confocal laser scanning microscope (Carl Zeiss, Germany).

2.8. Immunohistochemical analysis of ceramide in skin cross sections after WC treatment

The hair on the back skin of Balb/c mice was clipped, and treatment with WC (0.34 mA/cm^2, 1 hr) was performed on the skin by Ag/AgCl electrodes placed on absorbent cotton containing PBS. After 12 hr, the skin was collected, and soaked in 4% PFA for 1 hr at 4 °C. The skin was then soaked in 30% sucrose in PBS at 4 °C overnight. The skin was embedded in a freezing block of optimal cutting temperature (OCT) compound, and a cross section (10 μm) of the skin was prepared. Cross sections of skin were washed twice with PBS for 5 min, and then treated with blocking solution (3% BSA in PBS containing 50 μl of 0.1% Triton-X) for 1 hr at room temperature. Cross sections were washed an additional three times with PBS for 2 min. After washing, cross sections were treated with the primary antibody solution containing mouse anti-ceramide IgM (4 μg/ml in 1% BSA-PBS) at 4 °C. After 18 hr of incubation, skin

cross sections were washed three times with PBS for 2min., and then incubated in a solution of the secondary antibody containing goat anti-mouse IgG labeled with Alexa Fluor 488 (4 μg/ml in 1% BSA-PBS) at room temperature for 30 min, and washed three-times with PBS for 2 min. Nuclei were stained by incubating the skin cross sections overnight in the presence of DAPI solution, and observed with an LSM700 confocal laser scanning microscope (Carl Zeiss, Germany).

2.8. Statistical analysis

Statistical analysis was performed using one-way ANOVA followed by the Tukey–Kramer honest significant difference (HSD) test. *P* values <0.05 were considered to be significant, and were evaluated using KaleidaGraph (Hulinks Inc., Japan).

3. Results and Discussion

We previously evaluated the uptake of siRNA (MW: ca.12,000), CpG oligo DNA (MW: ca. 6,600), in-stem molecular beacon (ISMB) (MW: ca. 12,000), which fluoresces upon binding to target mRNA, and an intelligent shRNA expression device (iRed) (MW: ca. 200,000) upon treatment with WC (Kigasawa, et al., 2010; Kigasawa, et al., 2011; Hasan, et al., 2016a, b). We found that ISMB emitted fluorescence following treatment of cells with WC, suggesting that macromolecules taken up by WC-mediated endocytosis could escape from endosomes (Hasan, et al., 2016b). However, it's unclear whether the macromolecules were taken up during WC treatment.

We sought to quantitatively evaluate cellular uptake of macromolecules following WC treatment. Fluorescent dyes or fluorescence-labeled materials, such as dextran, are typically used for evaluation of the amount of cellular uptake. However, autofluorescence of cells prevents accurate quantification using fluorescence measurements. Therefore, PCR measurement of DNA was employed in the present study for accurate quantification of WC-mediated cellular uptake. We first used plasmid DNA encoding luciferase as a macromolecule for quantification of the amount of cellular uptake. However, luciferase DNA was not detected by real-time PCR following WC treatment (data not shown). It's possible that the MW of the plasmid DNA (ca. 3,500,000)

may have exceeded the size threshold that can be taken up by WC-mediated endocytosis. Next, we prepared smaller molecular weight DNA fragment encoding the luciferase open reading frame region (MW: ca. 99,000) by PCR using luciferase plasmid DNA as a template, and exposed the cells to WC treatment in the presence of the DNA fragment. Although the DNA fragment was not detected in the cells immediately following WC treatment (data not shown), the intracellular amount of the DNA fragment was detected at 1 hr after WC treatment, and the amount of the DNA fragment in cells increased significantly at 3 hr after WC treatment (Fig. 1). These results suggest that WC can induce endocytosis. Drug delivery efficiency is generally thought to be related to the current intensity of WC. However, we previously optimized the current intensity (0.34 mA/cm^2) based on *in vivo* experiments (Kigasawa et al., 2010). Treatment with higher current intensity (0.5 mA/cm^2) was found to induce inflammation on the surface of the skin. Furthermore, we previously found that WC induces de-polymerization of actin cytoskeleton (Hama et al., 2014). As a result of these effects, cells are easily detached from the culture dish upon treatment with higher current intensity *in vitro*, making it difficult to treat cells with higher current intensity (> 0.5 mA/cm^2) in an effort to optimize endosomal escape efficiency. Therefore, we used the previously identified optimized current intensity conditions used in the present study.

We then sought to confirm the functionality of high molecular weight proteins following delivery to the cytoplasm by WC-mediated endocytosis, since we only evaluated the functionalities of nucleic acids in our previous reports (Kigasawa, et al., 2010; Kigasawa, et al., 2011; Hasan, et al., 2016a, b). In the present study, an antibody (MW: ca. 150,000) was used as a representative functional high molecular weight protein to demonstrate the utility of WC-mediated cytoplasmic delivery. Cells were treated with WC in the presence of anti-nuclear pore complex antibody. As the molecular weight of this antibody exceeds the size that can leak from endosomes induced by WC, we performed WC treatment in the presence of the lysosomotropic agent chloroquine. In our previous study, we used chloroquine to enhance the escape of functional nucleic acids, namely iRed (MW: ca. 200,000), of which molecular weight was over 70,000, from WC-induced endosomes (Hasan, et al., 2016b). Following WC treatment in the presence of the anti-nuclear pore complex antibody with chloroquine, immunohistochemical staining of cells was carried out using Alexa Fluor 488-labeled secondary antibody against anti-nuclear pore complex antibody. The cytotoxicity of chloroquine was evaluated at various concentrations as a potential side effect. As shown in Supplementary Fig. 1, cell viability was not affected by the presence of 10 μM chloroquine. Thus, side effects of chloroquine were not observed under the experimental conditions. Using confocal microscopy, we

observed green fluorescence at the nuclear membrane, indicating that the anti-nuclear pore complex antibody associated with the surface of the nucleus (Fig. 2). These results suggest that high molecular weight protein antibodies delivered into the cytoplasm by WC had escaped from endosomes and exhibited functional binding. Thus, WC treatment can be used without carriers to deliver not only nucleic acids but also high molecular weight proteins, although supporting materials such as chloroquine may be required for effective endosomal escape.

To confirm the morphological characteristics of endocytosis induced by WC, we performed WC treatment in the presence of PEGylated gold nanoparticles (100 nm, -50 mV), which were used for visualization of macromolecules taken up by WC-mediated endocytosis in the present study, and observed the cells after WC treatment by transmission electron microscopy (TEM). TEM images showed the presence of several gold nanoparticles in the endosomes (Figs. 3a1-a3), which exhibited elliptical shapes that differed from the spherical shape of typical endosomes, including clathrin-coated endosomes (El-Sayed and Harashima, 2013; Sandvig, et al., 2018). Furthermore, we also obtained images of the moment that endocytosis occurred following treatment with WC (Figs. 3b1-b3). The widths and depths of the endosomes were approximately 100-200 nm and 500 nm, respectively. Meanwhile, membrane protrusions indicative of the induction

of macropinocytosis were not observed, and the sizes of the endosomes were smaller than those of macropinosomes (> 1 μm) (El-Sayed and Harashima, 2013). These images suggest that WC-mediated endocytosis is not macropinocytosis or clathrin- or caveolae-dependent endocytosis, although WC-mediated cellular uptake of siRNA was significantly reduced by inhibitors of macropinocytosis (amiloride) and caveolae-mediated endocytosis (filipin) as shown in our previous study (Hasan, et al., 2016a).

Based on previous studies, we speculated that the WC-mediated endocytosis observed by TEM (Fig. 3) may be dependent on the GTPase regulator associated with focal adhesion kinase-1 (GRAF1) (Hansen and Nichols; 2009; Grant and Donaldson, 2009; El-Sayed and Harashima, 2013), although the endosome width was larger than that seen for GRAF1-dependent endocytosis (ca. 40 nm) (Lundmark, et al., 2008). GRAF1-dependent endocytosis can be inhibited by the amiloride derivative ethylisopropylamiloride (EIPA) (El-Sayed and Harashima, 2013). Further, the caveolae inhibitor filipin is a cholesterol-binding agent that can inhibit the functionality of lipid raft membrane domains, which are associated with GRAF1-dependent endocytosis (El-Sayed and Harashima, 2013). However, WC-mediated cellular uptake of siRNA was not inhibited by a high concentration sucrose solution that is known to inhibit clathrin-dependent endocytosis (Khalil, et al., 2006). Taken together with our previous findings

and the results of inhibitor experiments, we hypothesized that WC-mediated endocytosis is GRAF1-dependent (Hasan, et al., 2016a).

Previous studies demonstrated that siRNA knockdown of expression of GRAF1 and its co-factor Cdc42 could specifically inhibit GRAF1-dependent endocytosis (Lundmark, et al., 2008; El-Sayed and Harashima, 2013). Thus, to confirm whether WC-mediated endocytosis is GRAF1-dependent, we examined the effect of RNAi targeting GRAF1 and Cdc42 on WC-mediated cellular uptake of the DNA fragment encoding luciferase by B16-F1 cells (Fig. 1). Pre-transfection of anti-Cdc42 siRNA or anti-GRAF1 siRNA reduced the levels of Cdc42 and GRAF1 mRNA in B16-F1 cells to below 30% of that seen for non-transfected cells (Supplementary Fig. 2). However, contrary to our expectation, the increase in the amount of luciferase-encoding DNA fragment induced by WC was not reduced by siRNA against either Cdc42 or GRAF1 (Supplementary Fig. 2). We also examined the amount of Cdc42 protein, a key factor in GRAF1-dependent endocytosis, in cells after WC treatment by western blotting with an anti-Cdc42 antibody. Results showed that WC treatment did not affect the amount of Cdc42 protein or Cdc42 phosphorylation, which inhibits Cdc42 function (Kwon, et al., 2000) (data not shown). More detailed analysis of the trigger mechanism of WC-mediated endocytosis is required in the future.

Next, we focused on the membrane characteristics of WC-induced endosomes, which leak macromolecules such as siRNA into the cytoplasm. Previous results suggested that WC treatment was responsible for the leakiness of the endosomal membrane. It has been reported that ceramide can form ceramide channels in the mitochondrial outer membrane, and that inter-membrane space proteins (MW: <60,000) are released from the mitochondria via ceramide channels (Perera, et al., 2016). Thus, we hypothesized that leakiness in the endosomal membrane was caused by localization of ceramide induced by WC treatment. To confirm this hypothesis, we examined the intracellular distribution of ceramide following WC treatment by immunostaining using an anti-ceramide antibody. Green fluorescence of anti-ceramide antibody was observed homogeneously in untreated cells (Control) (Figs. 4a-1 and 4a-2), which indicates that ceramide is indeed present in the cells. On the other hand, strong green fluorescent signals were observed in the cytoplasm as dots, which may be due to the presence of vesicular compartments, such as endosomes (Figs. 4b-1 and 4b-2). The fluorescence intensity of ceramide in each confocal laser scanning microscopic image of immuno-stained cells (Fig. 4a and b) was quantified using the image analysis software Image J. The difference between WC-treated and untreated groups was statistically significant ($p<0.01$), and the fluorescence intensity of the WC-treated group was 1.8-fold higher than that of the untreated group (Fig. 4c). These

results suggest that localization of ceramide changed from the cytoplasm to endosomes upon treatment with WC. Thus, endosomal properties are likely to be altered by localization of ceramide following WC treatment; this phenomenon may be responsible for the leakiness of WC-induced endosomes. It's possible that ceramide localized in endosomes results in the formation of pores that allow for macromolecules to leak through.

To obtain information regarding WC treatment-induced endocytosis, the vesicular compartment in the cells after WC treatment were stained with LysoTracker, which can stain acidic compartments such as endosome/lysosomes, after WC treatment of B16-F1 cells. As shown in Supplementary Fig. 3(a, b), the intensity of red fluorescence derived from LysoTracker was not so potent, and there was no colocalization with green fluorescence indicating ceramide. Probably, since the ceramide pore would prevent acidification by leakage of proton, the WC treatment-induced endosomes could not be stained with LysoTracker. Then, we tried to clarify whether the WC treatment-induced vesicular compartments are conventional endosomes by immunostaining of the cells after WC treatment with antibody against Rab7, which is known as a marker of conventional endosomes. As shown in Supplementary Fig. 3(c, d), red fluorescent signals of Rab7 did not co-localize with green fluorescent signals of ceramide. From this result, it was suggested that the ceramide rich vesicular compartments induced by WC treatment would

not be the conventional endosomes containing Rab7. Further investigations for identification of detail properties and component of ceramide rich vesicular compartments are required in the future.

To confirm whether the same phenomenon is observed *in vivo*, we performed WC treatment of mouse skin and used immunohistochemistry to evaluate the effect of WC on the skin distribution of ceramide, which would be a key factor in WC-mediated cytoplasmic delivery. As shown in Fig. 5, ceramide fluorescence in the cross section of the skin treated with WC was greater than that of untreated skin (Fig. 5a and b). In addition, the fluorescence intensity of WC-treated skin was 1.86-fold higher than that of untreated skin (Fig. 5c). These results confirm that ceramide is increased by WC treatment not only *in vitro*, but also in skin tissue *in vivo*. As we previously reported that *in vivo* WC treatment of siRNA on the skin showed significant gene knockdown (Kigasawa et al., 2010), macromolecules could be delivered to the cytoplasm by WC treatment even *in vivo*. Thus, results obtained by *in vivo* immunohistochemistry support the conclusion that localization of ceramide causes leakiness of endosomes induced by treatment with WC.

Furthermore, we examined the in vivo efficacy of WC treatment and cytoplasmic delivery of macromolecules using tumor-bearing mice. Regarding cytoplasmic delivery of macromolecules, we have already published the paper (Kigasawa, et al., 2010). In that

paper, we showed the significant mRNA knocking down by iontophoresis (WC treatment in vivo) of siRNA in the inflamed skin. The result is the evidence of the cytoplasmic delivery of macromolecules siRNA (MW:12,000) by WC in vivo, because the action site of siRNA is cytoplasmic space. Thus, significant RNAi effect indicates cytoplasmic delivery by WC in vivo. WC treatment with anti-glyceraldehyde-3-phosphate dehydrogenase (GAPDH) siRNA was performed on tumor-bearing mouse skin. As shown in Supplementary Fig. 4, mRNA level of GAPDH in tumor was significantly suppressed (37%) by WC treatment with anti-GAPDH siRNA. From this result, the WC treatment-mediated cytoplasmic delivery of macromolecules in vivo was confirmed by using tumor-bearing mice.

To obtain information regarding the role of ceramide and preferential localization of ceramide in WC-induced endosomes, we focused on neutral sphingomyelinase 2 and acid sphingomyelinase. Neutral sphingomyelinase 2 has been reported to localize to the plasma membrane, Golgi and recycling compartments (Airola, et al., 2013). On the other hand, acid sphingomyelinase localizes in lysosomes (Jenkins, et al., 2009). Thus, we expected that the source of ceramide would be identified by inhibition of ceramide synthesis with specific inhibitors against those sphingomyelinases. In this study, we used GW4869 and imipramine as specific inhibitors of neutral

sphingomyelinase 2 and acid sphingomyelinase, respectively (Airola, et al., 2013; Arenz, et al., 2010). The relative fluorescence intensity, which indicates the amount of ceramide in the cells following WC treatment with a neutral sphingomyelinase inhibitor GW4869, was slightly decreased, but the difference was not statistically significant (Supplementary Fig. 5a). In contrast, for the acid sphingomyelinase inhibitor imipramine, the amount of ceramide did not change (Supplementary Fig. 5b). These results suggest that WC did not activate ceramide synthesis. WC treatment may increase ceramide in the cells by inhibition of degradation or metabolic pathways. However, it was difficult to confirm the contribution of degradation/metabolic pathway inhibition in this study. Future studies are needed to clarify the mechanism of ceramide increase by WC and obtain direct evidence of ceramide pores; that may be responsible for endosomal escape of macromolecules.

The difference in the morphology of WC-induced endosomes from that of other endosomes may be the result of WC-induced endocytosis being a type of GRAF1-dependent tubular endocytosis, although pretreatment with siRNA against GRAF1 and cdc42 did not affect WC-mediated cellular uptake (Supplemental Fig. 1). Cellular uptake induced by WC treatment was previously shown to be inhibited by amiloride and filipin (Hasan et al., 2016a). Another possible reason for the tubular morphology of WC-induced endosomes may be due to localization of ceramide in the endosomes via WC treatment.

However, it is difficult to clarify the exact reason for the tubular morphology of WC-induced endosomes at this time.

In conclusion, we found that WC-mediated endocytosis occurred after treatment of cells with WC, and that WC treatment can trigger cellular uptake and cytoplasmic delivery of exogenous macromolecules. In addition, high molecular weight protein antibodies were functional following delivery into the cytoplasm mediated by WC in the presence of chloroquine. The WC-induced endosomes, which can leak macromolecules (MW: <70,000), exhibited elliptical shapes that differ from those of conventional endosomes, such as macropinosome, clathrin- or caveolae-dependent endosomes. Furthermore, ceramide was found to localize in endosomes following WC treatment. It is suggested that localization of ceramide may be cause of the leakiness of the endosomes induced by WC. Further investigations are necessary to better elucidate the exact mechanism of WC-mediated unique endocytosis.

Acknowledgements

This work was supported in part by JSPS KAKENHI Grant Number 18F18097 and

17H03976, and a Tokushima University research program for the development of an intelligent Tokushima artificial exosome (iTEX).

Declaration of interests

None.

Author Contributions

KKogure conceived and supervised the study, designed experiments, and wrote the manuscript; TShimokawa, NYamazaki, HAndo, TIshida, TFukuta and TTanaka supervised the study; TTorao, MMimura, YOshima, KFujikawa and MHasan performed experiments and analyzed data. All authors read and approved the final manuscript.

References

Airola, M.V., Hannun, Y.A., 2013. Sphingolipid metabolism and neutral sphingomyelinases. Handb. Exp. Pharmacol. 215, 57–76. https://doi.org/10.1007/978-3-7091-1368-4_3.

Arenz, C., 2010. Small Molecule Inhibitors of Acid Sphingomyelinase. Cell. Physiol. Biochem. 26, 1-8. https://doi.org/10.1159/000315100.

El-Sayed, A., Harashima, H., 2013. Endocytosis of gene delivery vectors: from clathrin-dependent to lipid raft-mediated endocytosis. Mol. Ther. 21, 1118-1130. https://doi.org/10.1038/mt.2013.54.

Grant, B. D., Donaldson, J. G., 2009. Pathways and mechanisms of endocytic recycling. Nat. Rev. Mol. Cell Biol. 10, 597-608. https://doi.org/10.1038/nrm2755.

Hama, S., Kimura, Y., Mikami, A., Shiota, K., Toyoda, M., Tamura, A., Nagasaki, Y., Kanamura, K., Kajimoto, K., Kogure, K., 2014. Electric stimulus opens intercellular spaces in skin. J. Biol. Chem. 289, 2450-2456. https://doi.org/10.1074/jbc.M113.514414.

Hansen, C. G., Nichols, B. J., 2009. Molecular mechanisms of clathrin-independent endocytosis. J. Cell Sci. 122, 1713-1721. https://doi.org/10.1242/jcs.033951.

Hasan, M., Nishimoto, A., Ohgita, T., Hama, S., Kashida, H., Asanuma, H., Kogure, K., 2016a. Faint electric treatment-induced rapid and efficient delivery of extraneous hydrophilic molecules into the cytoplasm. J. Control. Release. 228, 20-25.

https://doi.org/10.1016/j.jconrel.2016.02.048.

Hasan, M., Tarashima, N., Fujikawa, K., Ohgita, T., Hama, S., Tanaka, T., Saito, H., Minakawa, N., Kogure, K., 2016b. The novel functional nucleic acid iRed effectively regulates target genes following cytoplasmic delivery by faint electric treatment. Sci. Technol. Adv. Mater. 17, 554-562. https://doi.org/10.1080/14686996.2016.1221726.

Hashim, I.I., Motoyama, K., Abd-Elgawad, A.E., El-Shabouri, M.H., Borg, T.M., Arima, H., 2010. Potential use of iontophoresis for transdermal delivery of NF-kappaB decoy oligonucleotides. Int. J. Pharm. 393, 127-134. https://doi.org/10.1016/j.ijpharm.2010.04.020.

Jenkins, R.W., Canals, D., Hannun, Y.A., 2009. Roles and Regulation of Secretory and Lysosomal Acid Sphingomyelinase. Cell Signal. 21, 836–846.

Kajimoto, K., Yamamoto, M., Watanabe, M., Kigasawa, K., Kanamura, K., Harashima, H., Kogure, K., 2011. Noninvasive and persistent transfollicular drug delivery system using a combination of liposomes and iontophoresis. Int. J. Pharm. 403, 57-65. https://doi.org/10.1016/j.ijpharm.2010.10.021.

Kalia, Y. N., Naik, A., Garrison, J., Guy, R. H., 2004. Iontophoretic drug delivery. Adv Drug Deliv Rev. 56, 619-658. https://doi.org/10.1016/j.addr.2003.10.026.

Karpiński, T. M., 2018. Selected Medicines Used in Iontophoresis. Pharmaceutics 10, pii:

E204. https://doi.org/10.3390/pharmaceutics10040204.

Khalil, I. A., Kogure, K., Akita, H., Harashima, H., 2006. Uptake pathways and subsequent intracellular trafficking in nonviral gene delivery. Pharmacol. Rev. 58, 32-45. https://doi.org/10.1124/pr.58.1.8.

Kigasawa, K., Kajimoto, K., Hama, S., Saito, A., Kanamura, K., Kogure, K., 2010. Noninvasive delivery of siRNA into the epidermis by iontophoresis using an atopic dermatitis-like model rat. Int. J. Pharm. 383, 157-160. https://doi.org/ 10.1016/j.ijpharm.2009.08.036.

Kigasawa, K., Kajimoto, K., Nakamura, T., Hama, S., Kanamura, K., Harashima, H., Kogure, K., 2011. Noninvasive and efficient transdermal delivery of CpG-oligodeoxynucleotide for cancer immunotherapy. J. Control. Release. 150, 256-265. https://doi.org/ 10.1016/j.jconrel.2011.01.018.

Kwon, T., Kwon, D. Y., Chun, J., Kim, J. H., Kang, S. S., 2000. Akt protein kinase inhibits Rac1-GTP binding through phosphorylation at serine 71 of Rac1. J. Biol. Chem. 275, 423-428. https://doi.org/10.1074/jbc.275.1.423.

Labala, S., Jose, A., Chawla, S.R., Khan, M.S., Bhatnagar, S., Kulkarni, O.P., Venuganti, V.V.K., 2017. Effective melanoma cancer suppression by iontophoretic co-delivery of STAT3 siRNA and imatinib using gold nanoparticles. Int. J. Pharm. 525, 407-417.

https://doi.org/10.1016/j.ijpharm.2017.03.087.

Liu, K.C., Green, C.R., Alany, R.G., Rupenthal, I.D., 2013. Synergistic effect of chemical penetration enhancer and iontophoresis on transappendageal transport of oligodeoxynucleotides. Int. J. Pharm. 441, 687-692. https://doi.org/10.1016/j.ijpharm.2012.10.027.

Lundmark, R., Doherty, G. J., Howes, M. T., Cortese, K., Vallis, Y., Parton, R. G., McMahon, H. T., 2008. The GTPase-activating protein GRAF1 regulates the CLIC/GEEC endocytic pathway. Curr. Biol. 18, 1802-1808. https://doi.org/10.1016/j.cub.2008.10.044.

Patel, M.P., Churchman, S.T., Cruchley, A.T., Braden, M., Williams, D.M., 2013. Delivery of macromolecules across oral mucosa from polymeric hydrogels is enhanced by electrophoresis (iontophoresis). Dent. Mater. 29, e299-e307. https://doi.org/10.1016/j.dental.2013.09.003.

Perera, M. N., Ganesan, V., Siskind, L. J., Szulc, Z. M., Bielawska, A., Bittman, R., Colombini, M., 2016. Ceramide channel: Structural basis for selective membrane targeting. Chem. Phys. Lipids. 194, 110-116. https://doi.org/10.1016/j.chemphyslip.2015.09.007.

Sandvig, K., Kavaliauskiene, S., Skotland, T., 2018. Clathrin-independent endocytosis:

an increasing degree of complexity. Histochem. Cell Biol. 150, 107-118. https://doi.org/10.1007/s00418-018-1678-5.

Figure legends

Figure 1. Cellular uptake of DNA fragments after WC treatment.

The amount of intracellular DNA fragment taken up by B16-F1 cells was measured by real-time PCR of samples taken from untreated cells (white column) and those from cells taken 1 hr and 3 hr after WC treatment (black columns). Data are mean ± S.D (n=4). *p<0.005, vs. 1 hr WC(-) and 3hr WC(-), **p<0.001, vs. 1 hr WC(-), 1 hr WC(+) and 3 hr WC(-).

Figure 2. Immunostaining images of B16-F1 cells after WC treatment in the presence of anti-nuclear pore complex protein antibody.

WC treatment was performed in the presence of anti-nuclear pore complex protein antibody and chloroquine. After WC treatment, B16-F1 cells were subjected to immunostaining with an Alexa Fluor 488-labeled secondary antibody and observed by confocal laser scanning microscopy: (a) Alexa Fluor 488-labeled secondary antibody (green); (b) transmitted light image; (c) nuclei stained with DAPI (blue), and (d) merged image of cells without (WC(-)) or with WC treatment (WC(+)). The scale bar indicates 20 μm.

Figure 3. Transmission electron microscopy of cells after WC treatment in the presence of PEGylated gold nanoparticles.

B16-F1 cells were fixed 4 hr after WC treatment with gold nanoparticles, and cross-sections of the cells were observed by transmission electron microscopy. Gold nanoparticles (100 nm diameter) are indicated by white arrows and the scale bar indicates 1,000 nm. Panels a-2 and b-2 show magnified images of the square enclosed by dotted white lines in a-1 and b-1. Endosomes are indicated by the dotted white lines in a-3 and b-3.

Figure 4. Immunostaining images of B16-F1 cells using anti-ceramide antibody after WC treatment

After WC treatment, B16-F1 cells were subjected to immunostaining with anti-ceramide antibody and an Alexa Fluor 488-labeled secondary antibody, and observed by confocal laser scanning microscopy: (a) untreated cells (WC(-)) and (b) cells subjected to WC treatment (WC(+)). Panels a-2 and b-2 show magnified images of the square enclosed by the dotted white lines in a-1 and b-1. Green indicates Alexa Fluor 488-labeled secondary antibody and blue indicates nuclei stained with DAPI. The scale bar indicates 20 μm. (c)

Relative intensity of fluorescence of the cells quantified using the image analysis software Image J. Data are mean ± S.D (n>3). *p<0.01.

Figure 5. Immunohistochemical images of skin cross sections following WC treatment using anti-ceramide antibody

Following WC treatment of mouse skin, cross sections of the skin were subjected to immunohistochemistry with anti-ceramide antibody and an Alexa Fluor 488-labeled secondary antibody, and observed by confocal laser scanning microscopy: (a) untreated skin (WC(-)) and (b) skin subjected to WC treatment (WC(+)).Green indicates Alexa Fluor 488-labeled secondary antibody and blue indicates nuclei stained with DAPI, respectively. The scale bar indicates 20 μm. (c) Relative fluorescence intensity of skin cross sections quantified using the image analysis software Image J. Data are mean ± S.D (n=3). *p<0.05.

Figure 1

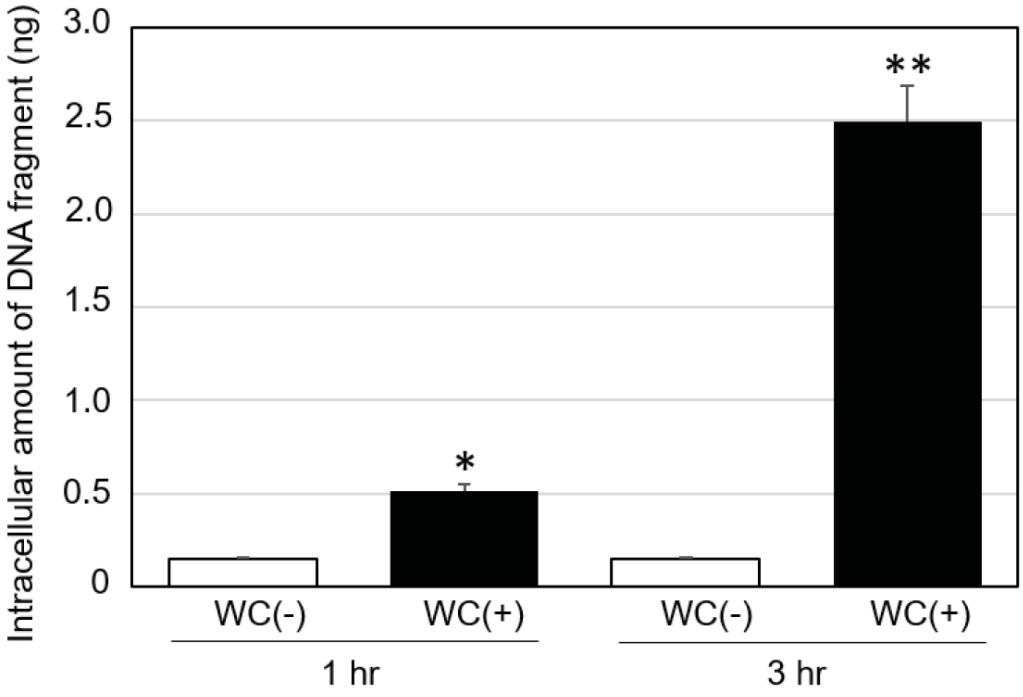

Figure 2

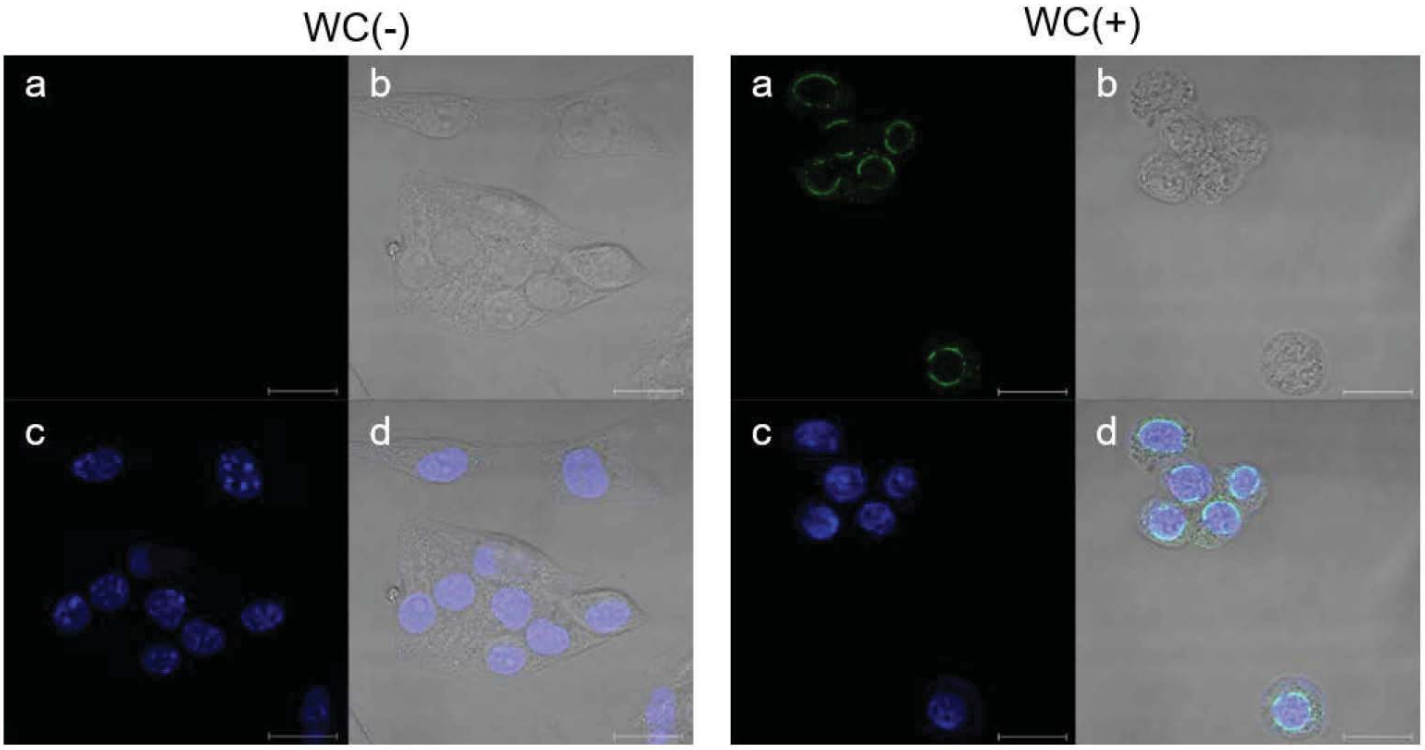

Figure 3

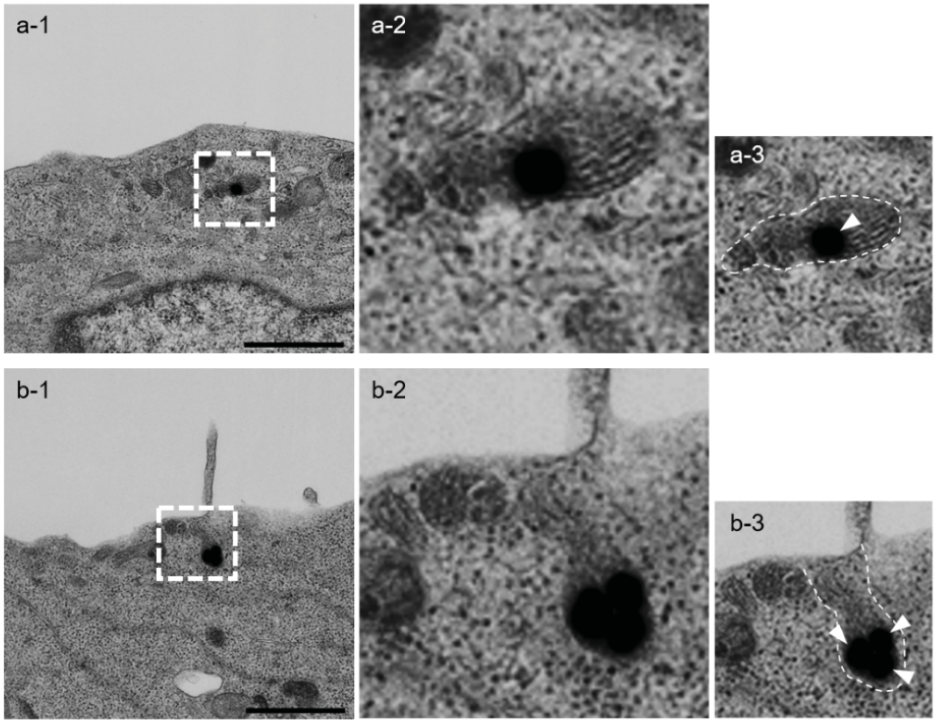

Figure 4

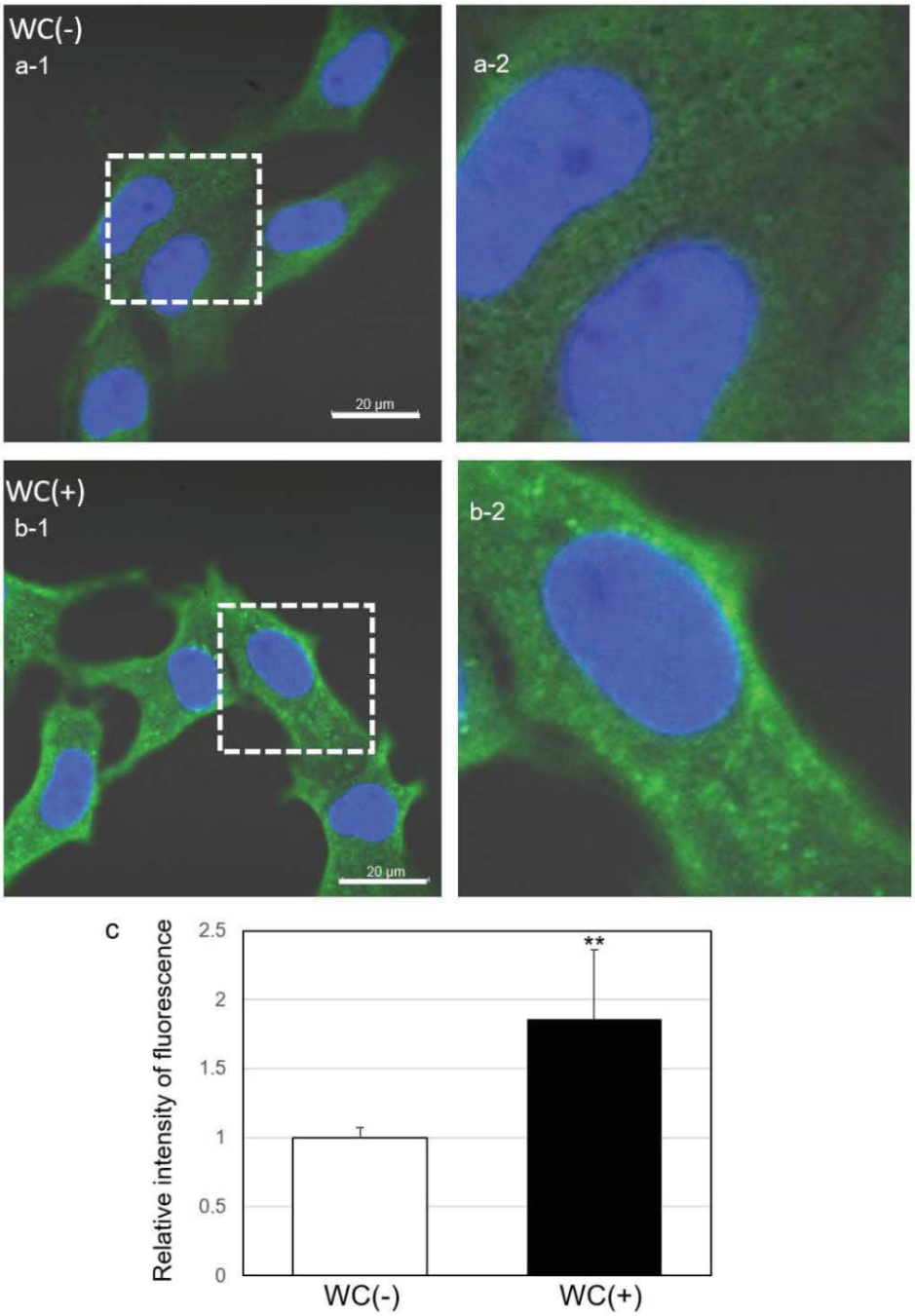

Figure 5

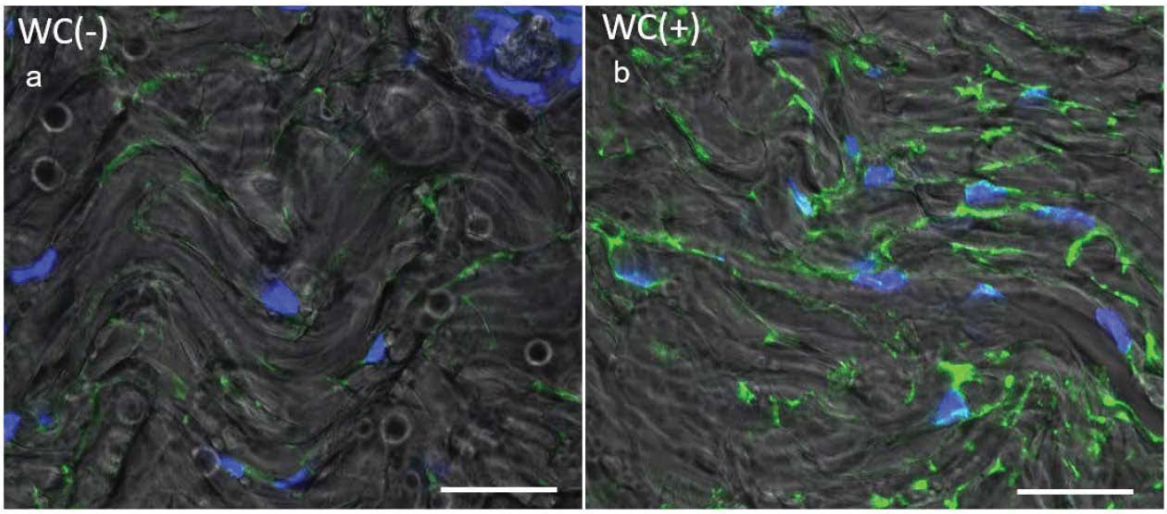
WC(-)
a
WC(+)
b

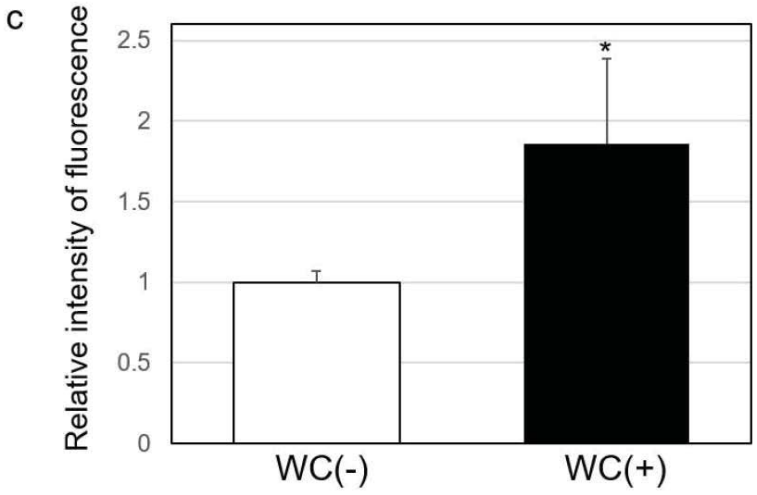
c
Relative intensity of fluorescence
2.5
2
1.5
1
0.5
0
*
WC(-)
WC(+)

Supplementary figure 1

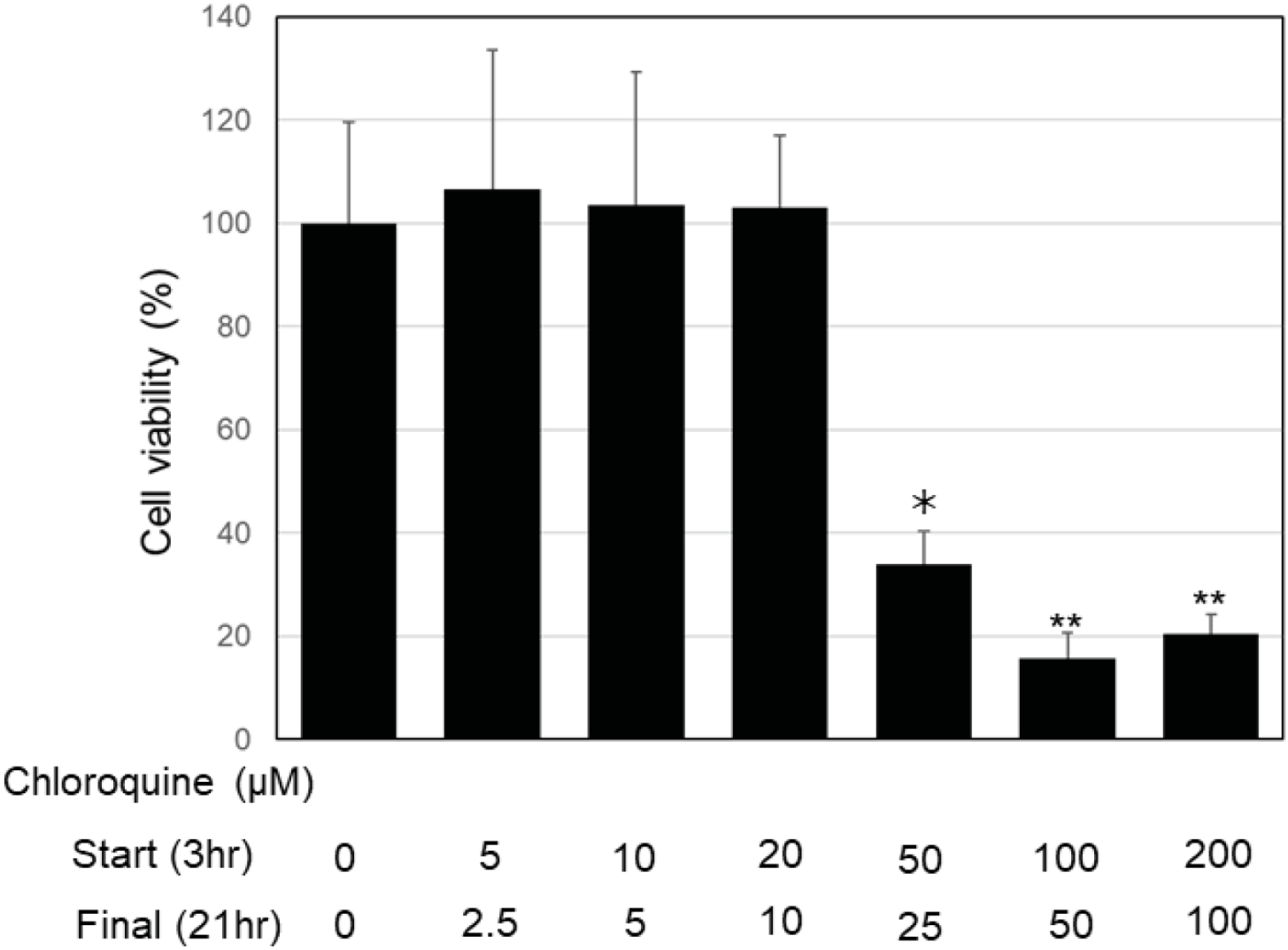

Supplementary figure 1. Effect of chloroquine treatment on cell viability

B16-F1 cells were incubated for 3 hr at 37 °C with various concentration of chloroquine before 1 ml DMEM containing 10% FBS was added to the cell dish for 21 hr. The concentration of chloroquine at start (earlier 3 hr incubation) was diluted to half at final (later 21 hr incubation). After incubation, the cells collected by trypsin treatment, and cell number stained with trypan blue was counted. *$p<0.05$, **$p<0.01$ vs control (chloroquine 0 μM)

Supplementary figure 2

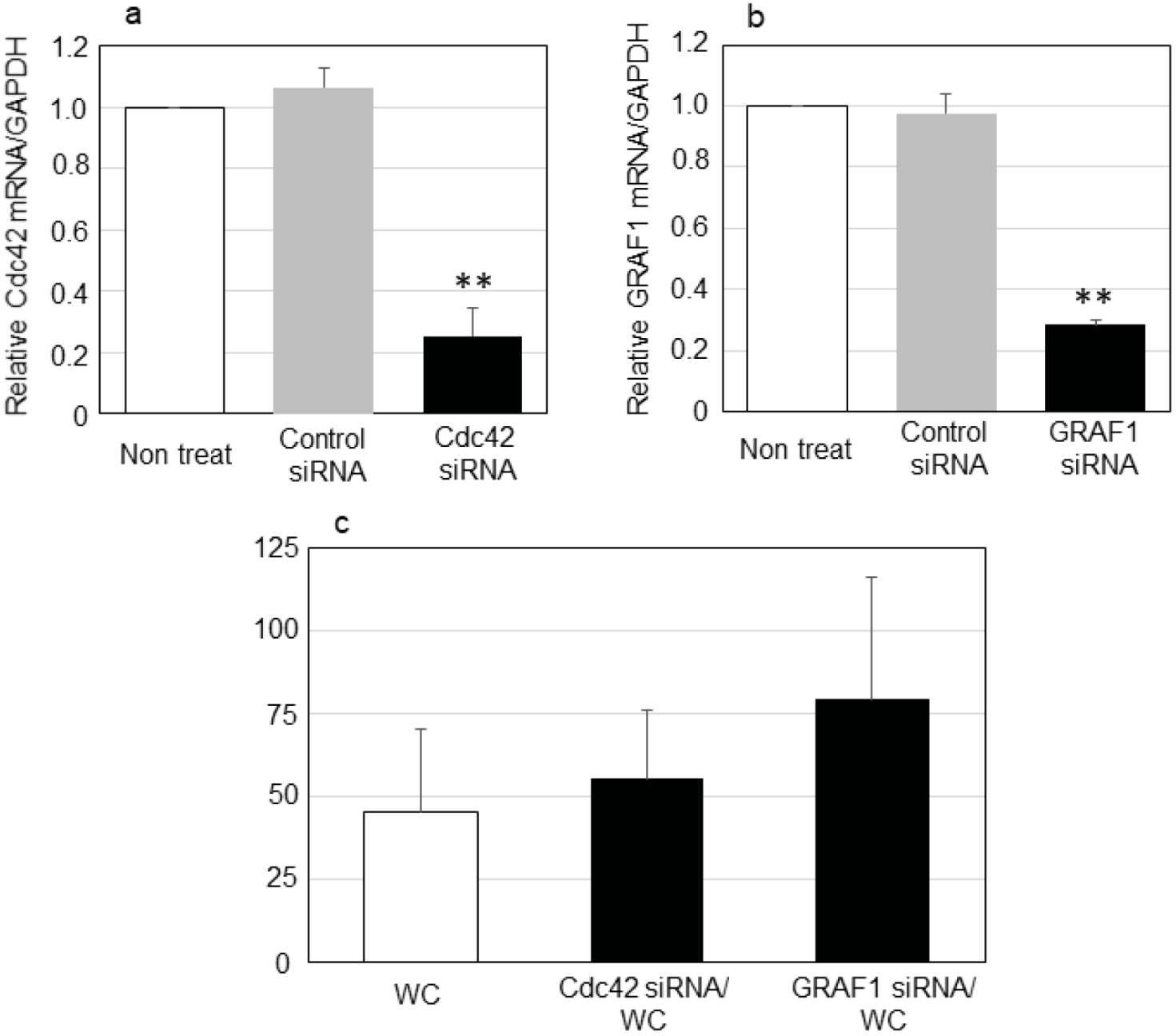

Supplementary figure 2. WC-mediated cellular uptake following siRNA-mediated Cdc42 and GRAF1 knockdown.

(a, b) RT-PCR measurement of Cdc42 and GRAF1 mRNA knockdown by siRNA transfection of B16-F1 cells. The amount of mRNA was measured by RT-PCR. (c) RT-PCR to determine the relative amount of intracellular DNA fragments after WC treatment of cells pretreated with siRNA against Cdc42 and GRAF1. WC treatment in the presence of DNA fragment was performed 24 hr after siRNA transfection. Data are means ± S.D. (n=3). Statistical significance at ** $p<0.001$, vs. Non treat and control siRNA.

Methods: B16-F1 cells (3.0 x 10^5 cells) were seeded into 35-mm dishes, and incubated at 37 °C for 24 hr. The cells were washed with PBS and resuspended in a solution containing Opti MEM, siRNA and Lipofectamine 3000, which was prepared according to the company's protocol. After 3 hr incubation at 37 °C, 1 mL DMEM containing 10% FBS was added to the dish, and the cells were incubated for 21 hr at 37 °C. Knockdown of GRAF1 or Cdc42 mRNA expression was confirmed by real-time PCR. After WC treatment with DNA fragment, B16-F1 cells were incubated at 37 °C for 1 hr or 3 hr and cellular DNA was extracted using a GenElute Mammalian Genomic DNA Miniprep Kit (Sigma-Aldrich, St. Louis, MO). The amount of DNA was quantified based on a calibration curve of the DNA fragment amplified using a real-time PCR Thermal Cycler Dice Real Time System Ⅲ (Takara Bio Inc., Japan) as mentioned in Materials and methods.

Supplementary figure 3

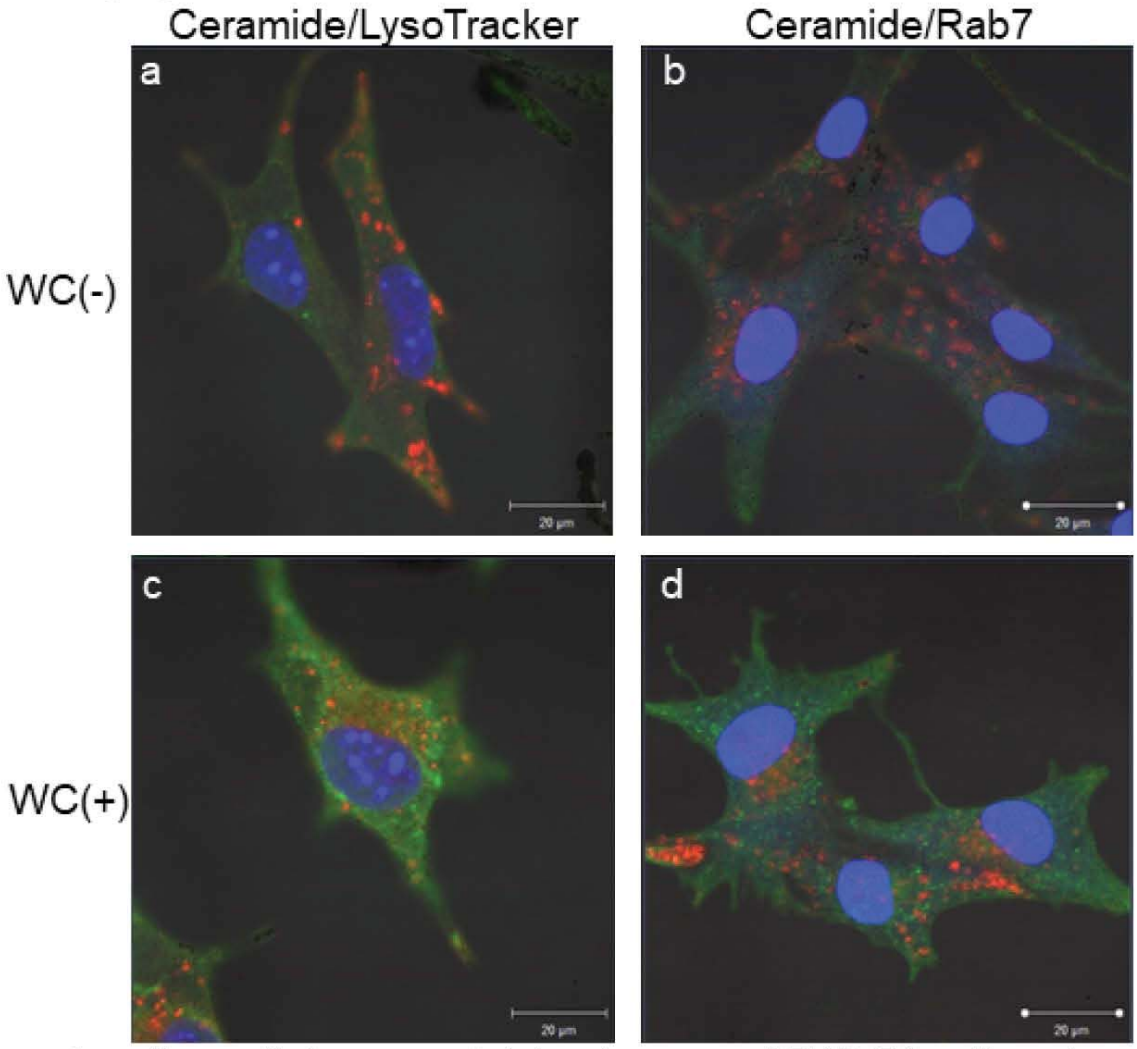

Supplementary figure 3. Immunostaining images of B16-F1 cells using anti-ceramide antibody and LysoTracker/anti-Rab7 antibody after WC treatment

(a) untreated cells and (c) WC-treated cells stained with anti-ceramide antibody/LysoTracker, and (b) untreated cells and (d) WC-treated cells stained with anti-ceramide antibody/anti-Rab7 antibody. Green indicates Alexa Fluor 488-labeled secondary antibody, red indicates LysoTracker (a, b)/Alexa Fluor 647 secondary antibody (c, d) and blue indicates nuclei stained with DAPI. The scale bar indicates 20 μm.

Method: Following treatment with WC (0.34 mA/cm^2, 15 min), B16-F1 cells were incubated for 24 hr at 37 °C. For staining endosome/lysosomes, LysoTracker solution was added, and the cells were incubated for 2 hr. The cells were then washed with PBS. PBS (0.5 ml) containing 4% PFA was added and the cells were incubated for 20 min at 37 °C. The cells were washed three times with PBS containing 1% BSA and 0.1% Triton. After washing, the cells were incubated for an additional 20 min at 37 °C in the presence of PBS containing 1% BSA and 0.1% Triton. Then, the cells were washed with PBS containing 1% BSA. PBS containing 1% BSA and the primary antibody (mouse anti-ceramide IgM and anti-Rab7 IgG) was added to the cells, and the cells were incubated for 1 hr at 37 °C. Following that, the cells were washed three times with PBS containing 1% BSA. Secondary antibody in 1%BSA-0.1%Triton-PBS was then added to the dish, and the cells were incubated for 1 hr at 37 °C. After incubation, the cells were washed three times with 1% BSA-0.1% Triton-PBS. Nuclei were stained by incubating the cells for 30 min in the presence of DAPI solution, and the cells were washed with PBS before observation with an LSM700 confocal laser scanning microscope (Carl Zeiss, Germany).

Supplementary figure 4

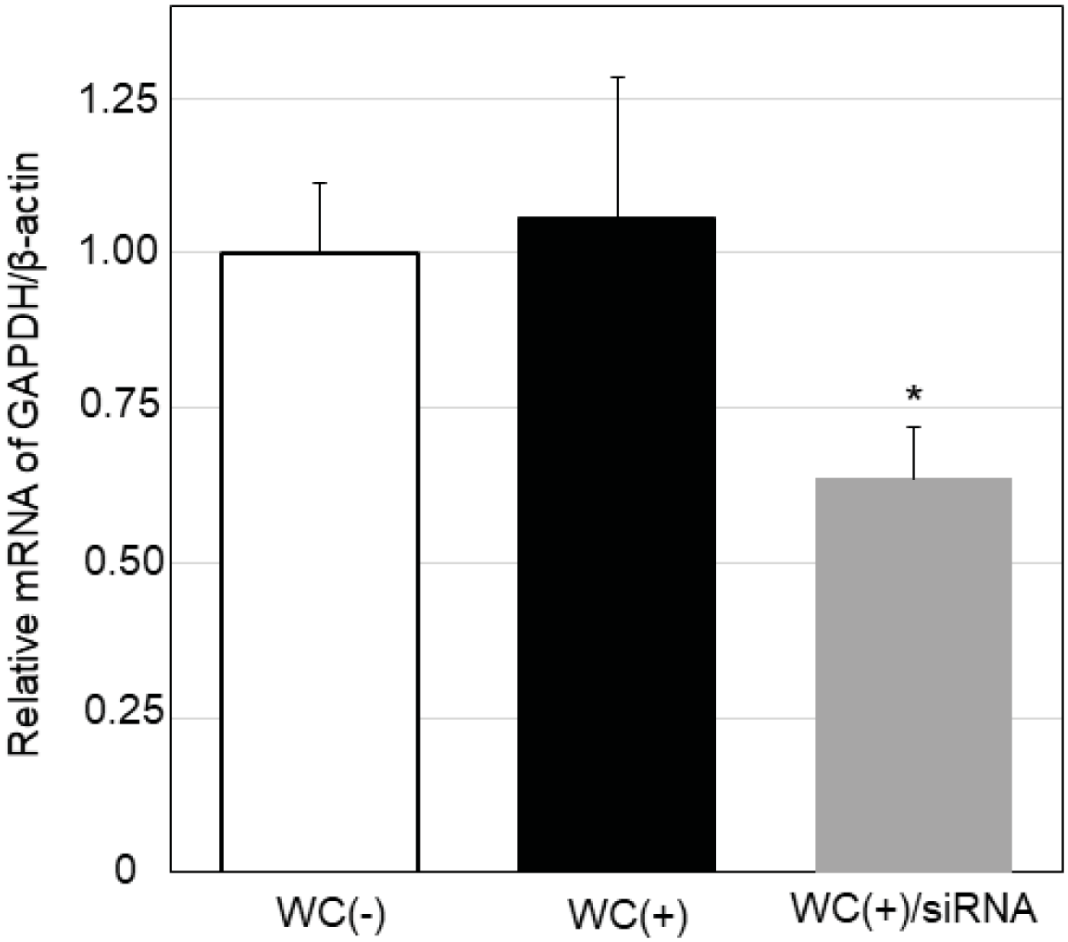

Supplementary figure 4. Effect of weak current treatment with anti-GAPDH siRNA on mRNA amount of GAPDH in tumor tissue of tumor bearing mice
Data are mean ± S.D (n>3). *p<0.05.

Method: For the preparation of mice bearing B16F1 melanoma, the B16-F1 cell suspension ($1X10^6$ cells) was mixed with ECM Gel (Sigma, St. Louis, MO, USA) at a ratio of 5:1 on ice (v/v), and cells were then inoculated under the skin of male C57BL/6J mice. After induction of the tumor (tumor volume 500-800 mm^3), the surface of the tumor was shaved and WC (0.34 mA/cm^2, 1 hr) was applied on the tumor by Ag/AgCl electrodes with absorbent cotton containing 10 μg anti-GAPDH siRNA in PBS. Total RNA was extracted from the tumor portion under the electrode after 24 hr of WC using an RNeasy Plus Mini kit (QIAGEN, Valencia, CA, USA) according to the manufacturer's instructions. cDNA was synthesized using PrimeScript RT Master Mix (Perfect Real Time, Takara Bio) and a MJ Mini Personal Thermal Cycler (BioRad Laboratories, Hercules, CA). Next, Real-time PCR was performed using TB Green Premix Ex Taq II (Tli RNaseH Plus) and a Thermal Cycler Dice Real Time System III (Takara Bio). β-Actin mRNA was used as an internal control. Relative mRNA expression was determined using the $2^{-\Delta\Delta CT}$ method.

Supplementary figure 5

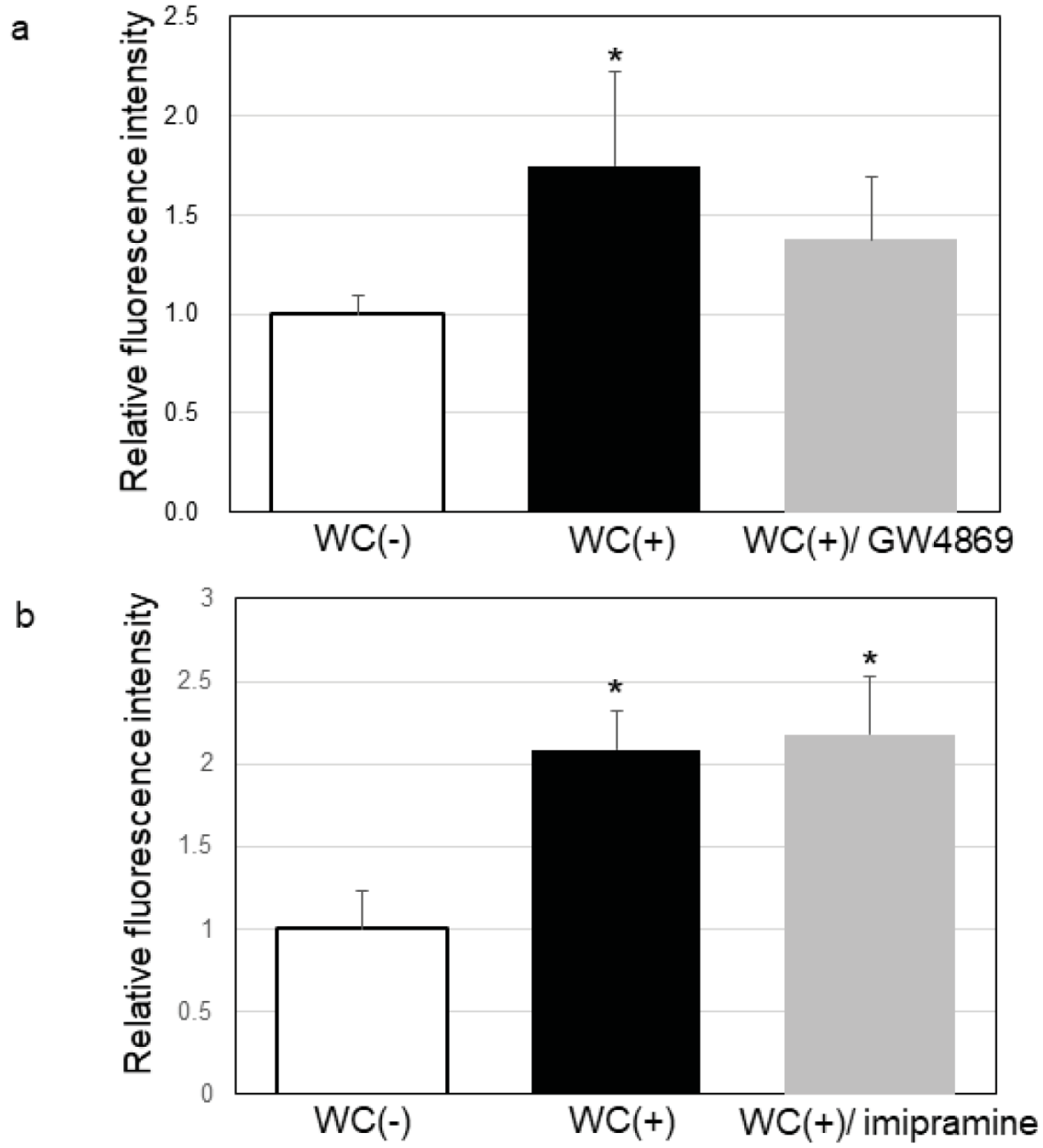

Supplementary figure 5. Effect of (a) an inhibitor of neutral sphingomyelinase GW4869 and (b) an inhibitor of acid sphingomyelinase imipramine on relative fluorescence intensity indicating ceramide amount

The B16-F1 cells were treated by WC with 5 μM GW4869 or 30 μM imipramine. After WC treatment, the cells were subjected to immunostaining with anti-ceramide antibody and an Alexa Fluor 488-labeled secondary antibody, and observed by confocal laser scanning microscopy Relative intensity of fluorescence of the cells quantified by image analysis software Image J. Data are mean ± S.D (n=6). *$p<0.01$, vs. Control.